Chemistry and Physics of Lipids 225 (2019) 104793

Contents lists available at ScienceDirect

Chemistry and Physics of Lipids

journal homepage: www.elsevier.com/locate/chemphyslip

Vibrational spectroscopy combined with molecular dynamics simulations as a tool for studying behavior of reactive aldehydes inserted in phospholipid bilayers

Danijela Bakarić[a], Dejana Carić[b], Katarina Vazdar[a], Mario Vazdar[a,*]

[a] Division of Organic Chemistry and Biochemistry, Ruđer Bošković Institute, Bijenička 54, HR-10000 Zagreb, Croatia
[b] Division of Physical Chemistry, Ruđer Bošković Institute, Bijenička 54, HR-10000 Zagreb, Croatia

ARTICLE INFO

Keywords:
Reactive aldehydes
Phospholipid bilayer
Vibrational spectroscopy
Magnetic resonance spectroscopy
Molecular dynamics simulations
Hydrogen bonding

ABSTRACT

Vibrational Fourier-transform infrared (FTIR) spectroscopy aided with molecular dynamics (MD) simulations is used for studying the interaction of several reactive aldehydes (RAs), nonanal (NA), 2-nonenal (NE), 4-hydroxy-2-nonenal (HNE) and 4-oxo-2-nonenal (ONE), with 1-palmitoyl-2-oleoyl-*sn*-glycero-3-phosphocholine (POPC) bilayer. The results obtained by the combination of these two techniques, supported also by electron paramagnetic resonance (EPR) spectroscopy, show that NA has the strongest stabilization in the bilayer, followed by less stabilized NE, HNE and ONE. We also revealed that HNE readily makes hydrogen bonds to carbonyl groups of POPC (but not to phosphate groups), in contrast to other RAs which are hydrogen bond acceptors and do not make hydrogen bonds with lipids. A combination of FTIR spectroscopy and MD simulations is sensitive to small chemical changes in the structures of RAs, thus making it a valuable tool for studying the weak interactions between compounds inserted to phospholipid bilayers.

1. Introduction

Reactive aldehydes (RAs), such as 4-hydroxy-2-nonenal (HNE) (Esterbauer et al., 1991) and 4-oxo-2-nonenal (ONE) (Seon Hwa et al., 2001), are constantly formed during oxidative stress (Catala, 2009) inside cellular membranes as a consequence of peroxidation of different polyunsaturated fatty acids (Yin et al., 2011). Due to their chemical structure, RAs easily react with neighboring lipids (Guichardant et al., 1998) and membrane proteins (Žarković et al., 2013) which leads to various irreversible covalent modifications of cellular membrane building matter. In normal physiological conditions inside living organisms, RAs are transported from the cellular membranes to the cytosol, where they are efficiently metabolized by glutathione-S-transferase and present no further harm to the organism (Catala, 2009). Low concentrations of covalently modified proteins are usually removed by the cellular proteasomal system and are not harmful in normal physiological conditions. However, if the concentration of modified proteins is too high, the removal of modified proteins is not efficient and this can lead to severe consequences and dangerous diseases (Grune and Davies, 2003).

In our previous work, we have analyzed the behavior of RAs with the principal aim of studying their reactivity to model peptides (Škulj et al., 2019) and lipids (Vazdar et al., 2017) in organic solvents as well as exploring the effect of chemically modified lipids on biophysical properties of phospholipid bilayers with embedded proteins (Jovanović et al., 2015). We have also studied the behavior of HNE in lipid bilayers by using molecular dynamics (MD) simulations and fluorescence spectroscopy where we have found out that HNE is relatively weakly stabilized in membranes and that transfer of HNE across cellular membranes occurs on a microsecond timescale, suggesting its active role in cell signaling pathway (Vazdar et al., 2012a). However, the molecular picture how RAs interact with individual phospholipid molecules is still missing. In order to examine this in more details, we employed vibrational Fourier-transform infrared spectroscopy (FTIR) which has been proven to be a suitable, probe-free choice for examining different molecular interactions in phospholipid bilayers (Fringeli and Günthard, 1981; Lewis and McElhaney, 2013; Tamm and Tatulian, 1997; Tatulian, 2003), in combination with MD simulations which are essential for characterization of the interactions in the bilayers at the atomistic level (Feller, 2000; Moradi et al., 2019; Tieleman et al., 1997). In addition, supporting experiments using electron paramagnetic resonance (EPR) spectroscopy useful in liposome characterization (Mirosavljević et al., 2014; Mirosavljević and Noethig-Laslo, 2008) were also performed.

Until today, FTIR has been successfully used in studying lipid phase

* Corresponding author.
E-mail address: mario.vazdar@irb.hr (M. Vazdar).

https://doi.org/10.1016/j.chemphyslip.2019.104793
Received 18 March 2019; Received in revised form 26 June 2019; Accepted 18 July 2019
Available online 29 July 2019
0009-3084/

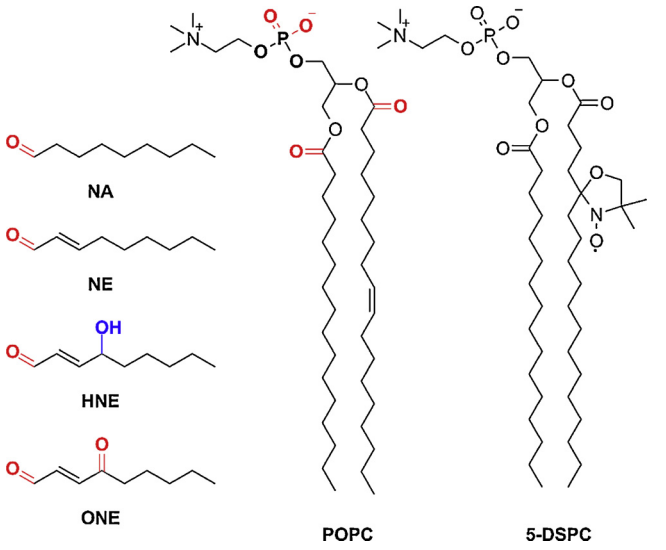

Fig. 1. Structures of reactive aldehydes, POPC and EPR spin probe 5-DSPC. Hydrogen bond donor groups (blue) and hydrogen bond acceptor groups (red) are shown for reactive aldehydes and POPC.

transition behavior in various lipid mixtures (Cieślik-Boczula et al., 2012; Kuć et al., 2015; Lewis et al., 1996; Mannock et al., 2006; Šegota et al., 2015a, 2015b; Veiga et al., 1999), and also for identification of hydrogen bonding patterns with polar groups of lipids, in particular phosphate and carbonyl groups (Casal et al., 1987; Choi and Swanson, 1995; Désormeaux et al., 1992; Díaz et al., 2003; Grdadolnik and Hadži, 1993; Gruenbaum and Skinner, 2011). However, to the best of our knowledge, FTIR spectroscopy has not been used so far to systematically study intermolecular interactions of a series of chemically different RAs with phospholipid bilayers.

In this work, we focus on the molecular fingerprint of the interaction of different RAs, in particular nonanal (NA), 2-nonenal (NE), 4-hydroxy-2-nonenal (HNE) and 4-oxo-2-nonenal (ONE) (Fig. 1), with 1-palmitoyl-2-oleoyl-*sn*-glycero-3-phosphocholine (POPC) bilayers. These aldehydes were strategically chosen to study primarily the influence of polar groups of RAs with the polar phosphate and carbonyl groups of POPC bilayer. This is achieved by slowly increasing the complexity of RA polar part, at the same time keeping hydrophobic interactions of RA with the bilayer similar due to equally long RA hydrocarbon tails. We combine experimental spectroscopic data with molecular dynamics simulations with the aim of elucidating whether the small structural changes of RAs are sufficiently large to be observed and quantified by the combination of the described techniques.

2. Methods

2.1. Chemicals

1-Palmitoyl-2-oleoyl-*sn*-glycero-3-phosphocholine (POPC) was purchased from Sigma Aldrich (≥ 95%). Reactive aldehydes (RAs) nonanal (NA) and trans-2-nonenal (NE) were purchased from Sigma Aldrich (95% and 97% purity, respectively). NE was additionally purified by column chromatography using pethroleum ether: ethyl acetate = 10:1 as eluent. 4-hydroxynonenal (HNE) and 4-oxononenal (ONE) were prepared according to known literature procedures (Soulère et al., 2007; Zimmermann et al., 2017). Phosphate buffer (PB) of ionic strength 0.1 M and pH 7.4 was prepared from Na_2HPO_4 (Alfa Aesar ≥ 99.0% purity) and $NaHPO_4$ (Fluka, ≥ 99.0% purity). 1-palmitoyl-2-stearoyl-(5-doxyl)-*sn*-glycerol-3-phosphocholine (5-DSPC, ≥ 99.0% purity) was purchased from Avanti Polar Lipids Inc. Chloroform ($CHCl_3$, p.a., stabilized with ethanol) and deuterium oxide (D_2O, 99% atom D) were obtained from, respectively, Lachner and Aldrich. Tetrachloroethene (C_2Cl_4, spectroscopic grade) was purchased from Acros Organics. All chemicals (except for NE) were used as received.

2.2. FTIR spectroscopy - preparation, spectra acquisition and spectral analysis of hydrated multilamellar supported lipid bilayers

Two sets of hydrated lipid films were prepared i) pure POPC and ii) POPC in the presence of RAs. In the former set, 10 mg of POPC was dissolved in 100 µL of $CHCl_3$. In the latter, 10 mg of POPC was dissolved in 100 µL of $CHCl_3$ along with RA ($m \approx 0.2$ mg). In such prepared solutions the molar ratio between the components was n(POPC):n(RA) = 10:1. Pure POPC lipids are measured in the liquid crystalline phase at $T = 37$ °C, as well as films of POPC + RAs where we assume that the film remains in the same phase due to relatively small concentration of added RA (Kim et al., 2013; Marinov and Dufourc, 1996). From each sample set 15–20 µL of lipid solution in $CHCl_3$ was taken and placed on one CaF_2 or BaF_2 window. After $CHCl_3$ evaporation at ambient temperature, the lipid film was formed. Residual traces of $CHCl_3$ were removed by placing the windows with the samples in a tube exposed to the N_2 current for about 5 min. After $CHCl_3$ was completely removed (checked by collecting the spectra of dry lipid films), the films were hydrated with D_2O as follows: a spacer of thickness $d = 6$ µm was fixed to the window with the film by using about 8 µL of D_2O. On the other window about 16 µL of D_2O was dropped. The windows were carefully assembled in a way that the entrance of air in a cell was prevented. The assembled cell was placed in a Harrick's temperature-controlled demountable liquid cell carrier. Additionally, RAs were dissolved in C_2Cl_4 ($c \approx 0.02$ mol dm^{-3}) in order to obtain FTIR spectrum of a single RA molecule surrounded with an inert nonpolar solvent.

FTIR spectra of hydrated lipid films were measured on an ABB Bomem MB102 spectrometer, equipped with CsI optics and DTGS detector. The assembled cell was heated from ambient temperature ($T = 25$ °C) to desired temperature ($T = 37$ °C) during 5 min; the system was held on $T = 37$ °C at least 5 min before the spectral acquisition started. Temperature was regulated by the refrigerated/heated circulator (Julabo, F12-ED). All spectra were collected with nominal resolution of 2 cm^{-1}, 20 scans and at $T = 37$ °C. Before taking the sample spectra, a background spectrum was recorded at the same conditions and automatically subtracted from the former in order to get atmosphere-free sample spectra.

In order to determine the position of a particular RA incorporated within a lipid bilayer, two spectral ranges are considered to be the most informative: i) carbonyl stretching (νC=O) region in which both POPC and RAs absorb and ii) the region in which antisymmetric stretching of phosphate groups ($\nu_{as}PO_2^-$) appears (Lewis and McElhaney, 2013). Both spectral regions (i: 1850-1400 cm^{-1} and ii: 1350-1000 cm^{-1}) were analyzed after a baseline correction in two ways: a) as raw spectra; b) as second derivative spectra. The latter was obtained after smoothing the raw spectra by the Savitzky-Golay procedure using Spectragryph v1.2.10 (Menges, 2018). Derivative spectroscopy (Wong and Mantsch, 1988) was employed because unambiguous determination of the position of carbonyl groups in raw FTIR spectra of RAs was partly prevented. In particular, an extensive overlap of the bands originated from the same functional groups (C=O) in different molecules (POPC and RAs) seriously disabled the determination of their position. Moreover, in pure POPC the C=O group make hydrogen bond (HB) with water so it is necessary to assume that one very strong band detected in this spectral range should be decomposed in minimally two bands: one attributed to the stretching of non-HB C=O group and another to the HB C=O group (Casal and Mantsch, 1984).

The same analogy is applied for the stretching of phosphate moieties. Since PO_2^- functional groups are strong HB acceptors, the analysis of this spectral range could provide an information about possible intermolecular interactions between polar head of POPC and RAs depending on the ability of the latter to form HB with the POPC phosphate group. Regarding the stretching of PO_2^- moieties, the antisymmetric

stretch is much more HB sensitive than the symmetric one which usually absorbs at about 1085 cm^{-1} (Hull et al., 2005). Therefore, the single band assigned as $\nu_{as}PO_2^-$ with a maximum at about 1220 cm^{-1}, can be decomposed into two bands: one as non-HB PO_2^- group and another as HB PO_2 group (Petrus et al., 2015).

As far as D_2O is concerned, it is used as a hydrating agent in order to avoid overlapping δ(HOH) band with ν(C=O) band. It is assumed that during short time of hydration (several minutes needed for spectra acquisition), substitution of D by H atoms from either POPC or RAs is neglected (Pawlikowska-Pawlęga et al., 2014).

2.3. EPR spectroscopy – preparation, spectra acquisition and spectral analysis of spin labeled unilamellar liposomes

In the first sample 10 mg of POPC was dissolved in 100 µl of $CHCl_3$. In all other samples 10 mg of POPC and RAs (m ≈ 0.2 mg) were mixed up in 100 µl $CHCl_3$ in ratio n(POPC):n(RAs) = 10:1. 5-DSPC probe was added as a solution in $CHCl_3$ in 0.1 mol% to all samples. The mixture was evaporated using a rotary evaporator and the resulting thin film was rehydrated using 100 µl of PB solution (0.1 M, pH 7.4). The obtained liposome dispersion was mechanically extruded through a 200 nm polycarbonate membrane (Whatman) about 150 times at room temperature.

EPR measurements were performed on *X*-band Varian E-109 spectrometer (10 GHz) equipped with a Bruker ER 041 XG microwave bridge and ER 4111 VT temperature unit. The data was collected at T = 37 °C using the supplied software (Morse, 1987). Spin labeled vesicles were measured in glass capillaries (inner diameter of 1 mm) applying the following instrumental setup: microwave power of 10 mW, modulation amplitude of 0.1 mT, modulation frequency of 100 kHz and scan range of 10 mT.

The order parameter S of the studied bilayers was calculated using EPR parameters A_{max} (mT) and A_{min} (mT), employing the following expression (Marsh, 1981).

$$S = \frac{3(A_{max} - A_{min})}{A_{max} + 2A_{min}} \times 0.5396$$

2.4. Molecular dynamics simulations

Molecular dynamics (MD) simulations were performed for POPC lipid bilayers containing 128 lipids arranged in two symmetrical leaflets with added 12 reactive aldehydes evenly distributed between the leaflets (NA, NE, HNE and ONE, Fig. 1) which roughly corresponds to the experimental ratio of n(POPC):n(RA) = 10:1 used in FTIR and EPR measurements. POPC lipids and RAs were described with SLipids force field (Jämbeck and Lyubartsev, 2012a, 2012b, 2012c). All missing bonding and non-bonding parameters of RAs were updated with compatible CHARMM36 parameters (Klauda et al., 2010) when needed. Atomic charges for RAs were calculated by the Merz-Singh-Kollman scheme (Singh and Kollman, 1984) which consists of B3LYP/6–31 G(d) geometry optimization, subsequent single point ESP charge calculation using B3LYP/cc-pVTZ method and a final atomic charge refinement with the RESP method (Bayly et al., 1993). All systems were solvated in a unit cell with ca. 11,000 TIP3P water (Jorgensen et al., 1983) molecules resulting in the size of approximately 6.5 × 6.5 x 12.0 nm. 3D periodic boundary conditions were employed with long-range electrostatic interactions beyond the non-bonded cut-off of 1 nm using particle-mesh Ewald procedure (Essmann et al., 1995) with a Fourier spacing of 0.12 nm. In all simulations, a semi-isotropic pressure coupling using Parrinello–Rahman algorithm (Parrinello and Rahman, 1981) was independently used in the directions parallel and perpendicular to the bilayer normal, maintaining pressure of 1 bar with a coupling constant of 10 ps^{-1}. All simulations were performed at 37 °C (310 K), the human body temperature often used in MD simulations of biological membranes, and controlled with the Nose–Hoover thermostat (Nosé, 1984) independently for the lipid and water subsystems using a coupling constant of 0.5 ps^{-1}. Bond lengths within the simulated molecules were constrained using the LINCS (Hess et al., 1997), whereas water bond lengths were kept constant employing the SETTLE method (Miyamoto and Kollman, 1992). Equations of motion were integrated using the leap-frog algorithm with a time step of 2 fs. Lipid bilayer membranes were initially equilibrated until a constant area per lipid was obtained (i. e. at least for 10 ns), followed with 200 ns of production used for analysis in unbiased simulations.

In order to calculate potential of mean force (PMF) for RAs across the POPC bilayer, we generated a set of initial configurations by pulling a center of mass of a single RA of interest along the bilayer z-axis from the final position obtained in unbiased MD simulations independently to water phase and to the bilayer center with the rate of 0.001 nm ps^{-1} and a harmonic restraint with a force constant of 1000 kJ mol^{-1} nm^{-2}. In this way, a set of 36 simulations with 0.1 nm spacing between them was generated, ranging from the bilayer center to the distance of 3.5 nm from the bilayer center in the water phase. Using the described set of initial configurations, we performed a series of 20 ns umbrella sampling simulations using a harmonic umbrella potential of 1000 kJ mol^{-1} nm^{-2}. First 1 ns was was discarded from the further analysis. Potential of mean forces were estimated from the biased distributions using the weighted histogram analysis method (WHAM) (Hub et al., 2010). The error bars in PMFs were calculated using the Bayesian bootstrap analysis with 100 bootstraps (Hub et al., 2010). MD simulations were performed with the GROMACS program package, version 5.1.4 (Abraham et al., 2015).

3. Results

3.1. FTIR spectra

A dominant spectral signature in raw spectra of hydrated multilamellar POPC bilayers in the carbonyl stretching region (1850-1400 cm^{-1}) (Fig. 2a) is the stretching of carbonyl groups of POPC ($\tilde{\nu}$ = 1737 cm^{-1}, indicated as $\nu(C=O_{POPC})$ in further text). Second derivative spectra of POPC bilayer reveals two maxima of $\nu(C=O_{POPC})$ at 1743 cm^{-1} and 1731 cm^{-1} (Fig. 2b) attributed to the stretching of non-hydrogen-bonded (non-HB, $\nu(C=O_{POPC\text{-}non\text{-}HB})$) and hydrogen-bonded (HB, $\nu(C=O_{POPC\text{-}HB})$) POPC carbonyl groups with interfacial water. Since the former band is more intense than the latter, there are more non-HB than HB C=O groups, indicating that water is not completely involved in hydrogen bonding with POPC carbonyl groups.

In raw spectra of POPC + RAs hydrated multilamellar bilayers $\nu(C=O_{POPC})$ band appears at $\tilde{\nu}$ = 1735 cm^{-1} (POPC + NA), $\tilde{\nu}$ = 1733 cm^{-1} (POPC + NE), $\tilde{\nu}$ = 1738 cm^{-1} (POPC + HNE) and $\tilde{\nu}$ = 1735 cm^{-1} (POPC + ONE). A small displacement to the low wavenumber region in POPC + NA, POPC + NE and POPC + ONE, as well as small displacement to the high-wavenumber region in POPC + HNE, occurs due to the change in the abundance of HB and non-HB C=O groups of POPC with water and RA depending on the nature of studied RA and its equilibrium position in the bilayer (Ryu et al., 2010). Importantly, due to the structure of studied RAs (Fig. 1), only HNE can serve as hydrogen bond donor to carbonyl groups with its −OH group, whereas other aldehydes are exclusively hydrogen bond acceptors (Fig. 1). The detailed analysis of the bands originated from carbonyl stretching of RAs in POPC + RAs system differs for various RAs and will be discussed in the following sections.

In raw spectra of POPC + NA hydrated multilamellar bilayers the band $\nu(C=O_{NA})$ generated by NA is not observed. This is not surprising since a single NA molecule (measured in C_2Cl_4) produces this signal at 1731 cm^{-1} which is largely overlapped with $\nu(C=O_{POPC})$ found at 1737 cm^{-1} (Fig. 2a). Second derivative spectrum reveals two maxima of at 1744 cm^{-1} and 1732 cm^{-1} (Fig. 2b), both of them attributed to POPC, in particular the $\nu(C=O_{POPC\text{-}non\text{-}HB})$ and $\nu(C=O_{POPC\text{-}HB})$ which look similar to neat POPC indicating no difference in hydrogen bonding

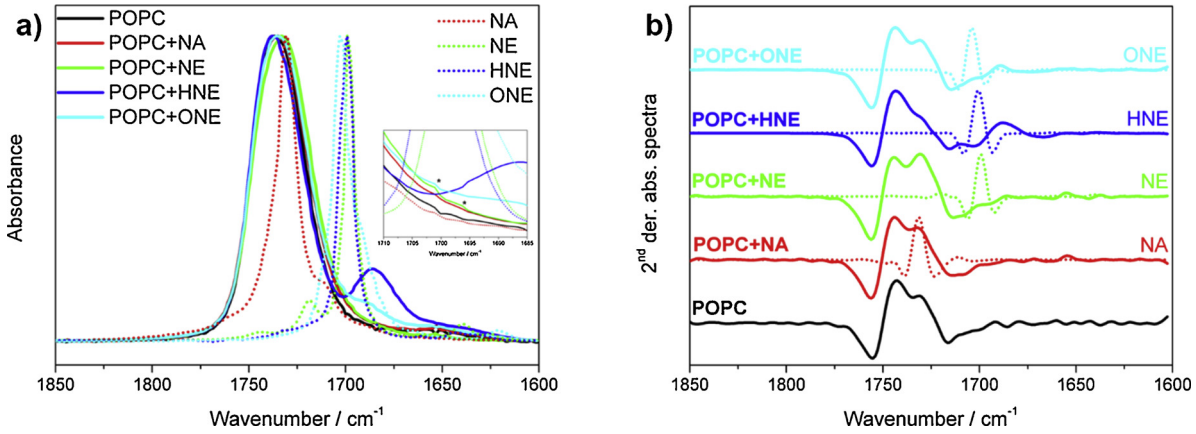

Fig. 2. Normalized FTIR spectra of hydrated multilamellar bilayers of POPC and POPC + RAs (NA, NE, HNE, ONE) obtained at 37 °C in spectral range 1850-1400 cm^{-1}: a) raw spectra; b) second derivative spectra. FTIR spectra of RAs dissolved in C_2Cl_4 are presented with dotted lines.

to water between these two systems. However, a very small displacement of $\nu(C=O_{POPC\text{-}HB})$ to higher wavenumbers in comparison with neat POPC bilayers is accompanied with the intensity gain of the signal at 1732 cm^{-1}, suggesting that $\nu(C=O_{NA})$ is hidden beneath it. Therefore, we can conclude that $\nu(C=O_{NA})$ of NA in POPC is not changed compared to C_2Cl_4, suggesting that carbonyl group of NA is located in the environment similar to nonpolar C_2Cl_4.

In POPC + NE system very weak bands at 1701 cm^{-1} and 1697 cm^{-1} are attributed to the $\nu(C=O)$ band of NE (Fig. 2a, see the augmented inset labeled with * and indicated as $\nu(C=O_{NE})$). Since $\nu(C=O_{NE})$ of a single NE molecule absorbs at 1699 cm^{-1} in C_2Cl_4, it follows that in POPC bilayers NE molecules are located in two slightly different arrangements – in one C=O bond of NE is shortened (1701 cm^{-1}) and another one in which this bond is elongated (1697 cm^{-1}) resulting from weak hydrogen bonding to interfacial water. Almost equal and very weak intensity of these bands, as well as the same displacement from the $\nu(C=O_{NE})$ band of a single NE molecule (± 2 cm^{-1}) implies an almost equal proportion of NE located in two different arrangements. A more detailed second derivative spectrum (Fig. 1b) demonstrates that the intensity of HB signal of $\nu(C=O_{POPC\text{-}HB})$ dominates (at 1731 cm^{-1}) in contrast to the non-HB $\nu(C=O_{POPC\text{-}non\text{-}HB})$ (at 1744 cm^{-1}), which differs from the neat POPC where signal from non-HB C=O groups dominates. Therefore, it seems that NE induces rearrangement of water and resulting in stronger hydrogen bonding between POPC carbonyl groups and interfacial water compared to neat POPC.

In POPC + HNE, a distinct band at 1685 cm^{-1} in raw spectra appears due to $\nu(C=O)$ of HNE (Fig. 2a, indicated as $\nu(C=O_{HNE})$) and can be clearly identified. In comparison with the spectrum of HNE in C_2Cl_4 $\tilde{\nu}$ = 1700 cm^{-1}) this band is displaced by 15 cm^{-1} to low wavenumber region, implying that C=O group in HNE participates in strong hydrogen bonding as hydrogen bond acceptor, either to interfacial water or another hydrogen bond donor. Since the hydrogen bonding to water occurs also for other RAs which are hydrogen bond acceptors and do not show a significant effect on the $\nu(C=O_{RA})$ stretching (see results for other RAs), it follows that the elongation of C=O bond is mainly due to interaction with another HNE molecule in the bilayer. However, hydroxyl −OH group of HNE, which is a part of the π delocalized system (Fig. 1), serves as a hydrogen bond donor towards POPC carbonyl group as well which in turn results in the intramolecular charge distribution in HNE leading to the slight elongation of C=O bond. A second derivative spectrum (Fig. 2b) suggests a decrease in the proportion of a HB C=O groups of POPC, $\nu(C=O_{POPC\text{-}HB})$ (1730 cm^{-1}) at the expense of non-HB groups, $\nu(C=O_{POPC\text{-}non\text{-}HB})$ (1743 cm^{-1}), indicating that water around POPC carbonyl group is expelled and replaced by HNE which seems to be not as optimal HB donor as water. Interestingly, this is different to the behavior of NE which induces stronger binding of POPC carbonyl groups to interfacial water. Finally, an additional signature in second derivative spectra is observed at $\nu(C=O_{HNE})$ at 1688 cm^{-1} and corresponds to the band observed in raw spectra at 1685 cm^{-1} attributed to hydrogen bonding to POPC carbonyl groups.

In the raw spectra of POPC + ONE, $\nu(C=O)$ of ONE produces a weak band at 1689 cm^{-1} and a very weak band at 1701 cm^{-1} (Fig. 2a, indicated as $\nu(C=O_{ONE})$). As ONE molecule possesses two carbonyl groups (aldehyde and keto group, Fig. 1), it is possible that these groups produce different signals in spectra. Both of them are displaced to the low wavenumber region in comparison with a single ONE molecule in C_2Cl_4 (1703 cm^{-1}), suggesting that C=O and HC=O bonds of ONE in POPC are elongated and participate in hydrogen bonding to surrounding water. More details are revealed from the second derivative spectrum (Figure 2b) – in addition to signatures of a non-HB, $\nu(C=O_{POPC\text{-}non\text{-}HB})$ (1744 cm^{-1}) and HB, $\nu(C=O_{POPC\text{-}HB})$ (1730 cm^{-1}) carbonyl groups of POPC which look similar to neat POPC and show no difference in hydrogen bonding to water, $\nu(C=O_{ONE})$ band appears at 1690 cm^{-1} (comparable to $\nu(C=O_{ONE})$ band at 1689 cm^{-1} in the raw spectrum) with a weak low frequency shift, additionally confirming that ONE participates in weak hydrogen bonding to interfacial water.

Raw spectra of hydrated multilamellar POPC and POPC + RAs in the spectral range 1350-1000 cm^{-1} exhibit several maxima of more or less overlapped bands. In contrast to carbonyl stretching which is present in both POPC and RAs, the most informative signal is the one originated from antisymmetric stretching of phosphate moieties of POPC ($\nu_{as}PO_2^-$) which maximum is commonly found at around 1232 cm^{-1} (Lewis and McElhaney, 2013). This band is party unresolved due to the signals from the wagging of − CH_2 − groups (Lewis and McElhaney, 2013), as well as from the bending od D_2O (at ca. 1210 cm^{-1}) (Pawlikowska-Pawlęga et al., 2014). Additional bands observed in spectral range 1350-1000 cm^{-1} are due to the symmetric stretching of phosphate groups ($\nu_{sym}PO_2^-$ at about 1085 cm^{-1}) and symmetric (ν_{sym}C-O appears at about 1070 cm^{-1},) and antisymmetric stretching (ν_{as}C-O appears at about 1170 cm^{-1} of POPC C-O groups. The latter three bands are considered to be insignificant in the elucidation of the interaction pattern made by lipid molecules (Lewis and McElhaney, 2007) so the discussion will be limited only to $\nu_{as}PO_2^-$.

Band maximum of $\nu_{as}PO_2^-$ in raw FTIR spectra appears at: 1237 cm^{-1} (POPC), 1236 cm^{-1} (POPC + NA), 1235 cm^{-1} (POPC + NE), 1238 cm^{-1} (POPC + HNE) and 1235 cm^{-1} (POPC + ONE), (Fig. 3a). In comparison with pure POPC, the presence of NA, NE and ONE slightly displaces the maxima to the lower wavenumber region, whereas HNE is placed in the opposite direction, but also by a very small amount (≈1 cm^{-1}). This indicates the ability of HNE to act as a hydrogen bond donor using −OH group, with phosphate moiety acting as hydrogen bond acceptor similar to hydrogen

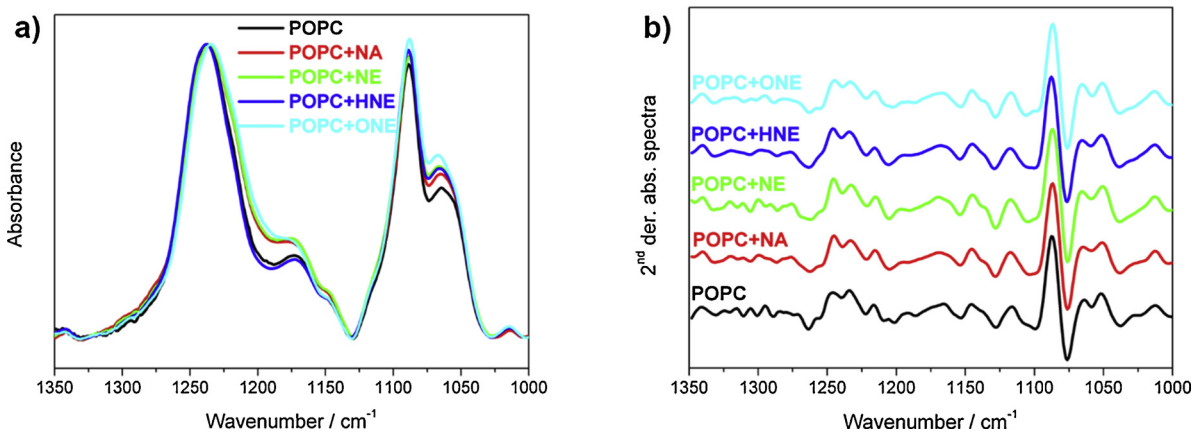

Fig. 3. Normalized FTIR spectra of hydrated multilamellar bilayers of POPC and POPC + RAs (NA, NE, HNE, ONE) in the spectral range 1350-1000 cm^{-1}: a) raw spectra; b) second derivative spectra.

bonding to POPC carbonyl groups. However, in contrast to carbonyl stretching, the detailed examination of second derivative spectra (Fig. 3b) reveals only very small variations in the positions of non-HB and a HB phosphate groups and far less details as compared to the carbonyl stretching region (Fig. 2b). Non-HB $\nu_{as}PO_2^-$ band appears at: 1246 cm^{-1} (POPC), 1245 cm^{-1} (POPC + NA), 1245 cm^{-1} (POPC + NE), 1246 cm^{-1} (POPC + HNE) and 1245 cm^{-1} (POPC + ONE); HB ν_{as} PO_2^- band appears at: 1234 cm^{-1} (POPC), 1234 cm^{-1} (POPC + NA), 1233 cm^{-1} (POPC + NE), 1234 cm^{-1} (POPC + HNE) and 1233 cm^{-1} (POPC + ONE), suggesting weaker interactions between RAs and POPC phosphate group. Moreover, the intensity of non-HB $\nu_{as}PO_2^-$ bands is stronger than intensity of HB ν_{as} PO_2^- bands in all systems, indicating that POPC phosphate group does not participate in hydrogen bonding in a large amount in contrast to POPC carbonyl group where the changes in the second derivative spectra are more pronounced.

3.2. EPR spectra

EPR spectra of hydrated unilamellar POPC and POPC + RAs liposomes recorded at $T = 37$ °C are presented in Fig. 4.

Values of the hyperfine splitting parameters $2A_{max}$ and $2A_{min}$ were determined from the raw spectra (Fig. 4). The analysis of the order parameter S shows that the largest disordering effect and in turn increase of lipid fluidity is the most pronounced for NA, whereas the effect for other aldehydes is smaller and roughly similar (Table 1). The relative change of the order parameter S for insertion of NA is

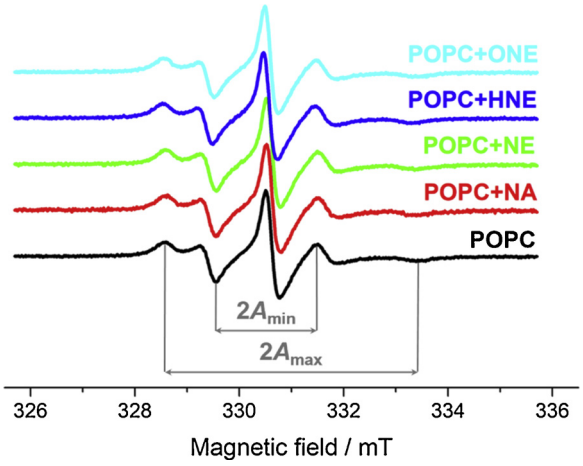

Fig. 4. EPR spectra of POPC and POPC + RAs (NA, NE, HNE, ONE) unilamellar liposomes labeled with 5-DSPC spin probe.

comparable to the effect of DOPE adducts with ONE (Jovanović et al., 2015) and fatty acids (Malingriaux et al., 2013). The increase of bilayer fluidity around the spatial position of 5-DSPC probe is the highest when NA is inserted, indicating that its residence time is the largest in the vicinity of the spin probe. The change in order parameter for other RAs is smaller and no large increase in bilayer fluidity in the vicinity of the 5-DSPC probe is observed.

3.3. Molecular dynamics simulations

Number density profiles for all studied RAs embedded in DOPC bilayer are shown in Fig. 5.

First, we see that the overall arrangement of phospholipid headgroups (shown as number densities of central atoms in choline, phosphate and carbonyl group in POPC) and water density distribution is almost identical in all systems as expected for relatively small concentration of RAs studied in this work. Importantly, the water density is significantly higher around phosphate groups (at distances of ca. 2 nm from the bilayer center) as compared to water density around carbonyl groups (at distances of ca. 1.5 nm from the bilayer center) demonstrating that phosphate groups are better solvated than carbonyl groups. Analysis of distribution of RAs in the bilayers reveals that NA has the largest density in the bilayer center, followed by NE, ONE and finally HNE (Fig. 5 a–d). On the other hand, HNE has the largest number density maximum which is located near phospholipid headgroups (Fig. 5c), followed by ONE, and NE and NA. Although these results are quite informative and are related to lipophilicity of studied RAs, it is not possible to connect it directly to relative stability of RAs in bilayer relative to water, since a small amount of HNE and ONE is found outside the bilayer in the water phase (Figs. 5c and 5d). Importantly, all studied RAs are inserted quite deep in the membrane, with the maximum number density just below POPC carbonyl groups (Fig. 5). The distribution of aldehydes is symmetric after 200 ns, as expected in the equilibrium. Due to the relatively low concentration of RAs (10 lipids:1 RA which results in only 12 lipids per 128 lipids in the bilayer in our MD simulations) we did not notice any flip flop event during 200 ns of MD simulations which would yield an asymmetric bilayer. However, we also do not expect that the difference in distribution of RAs between the leaflets would lead to different interactions with POPC. Within our setup, it is almost impossible to notice any difference in binding of RAs to POPC which is mainly of local character and is not influenced by global RA concentration.

In order to check for the relative stability of RAs in the bilayer, we performed free energy calculations using umbrella sampling. The obtained free energy profiles are shown in Fig. 6.

Based on the presented data, we see that stabilization of NA vs. bulk is ca. -6 kcal mol^{-1}, followed by NE (ca. -4 kcal mol^{-1}), HNE (ca.

Table 1
Values of the hyperfine splitting parameters $2A_{max}$ and $2A_{min}$ (in mT) for hydrated unilamellar liposomes of POPC and POPC + RAs and order parameter S calculated from it. Ratio S_x/S_0 is expressed in a way that S_0 was set to be 100, whereas other order parameters S_x is are expressed relative to this value.

	POPC	POPC + NA	POPC + NE	POPC + HNE	POPC + ONE
$2A_{min}$	1.953 ± 0.021	1.970 ± 0.020	1.963 ± 0.015	1.975 ± 0.007	1.977 ± 0.006
$2A_{max}$	4.833 ± 0.021	4.773 ± 0.021	4.823 ± 0.021	4.825 ± 0.007	4.857 ± 0.040
S	0.534 ± 0.003	0.521 ± 0.003	0.529 ± 0.004	0.526 ± 0.001	0.529 ± 0.004
S_x/S_0	100	97.6 ± 0.6	99.2 ± 0.8	98.6 ± 0.2	99.2 ± 0.8

-3.5 kcal mol^{-1}) and finally ONE (ca. -2.5 kcal mol^{-1}). In addition, we can also estimate the energy needed for flip flop of RAs, i. e. free energy needed for RAs to cross from one leaflet to another. Flip-flop free energy barrier is the smallest for NA (ca. 0.5 kcal mol^{-1}), followed by NE (ca. 1 kcal mol^{-1}), ONE (ca 1.5 kcal mol^{-1}) and the largest for HNE (ca. 2 kcal mol^{-1}). The present results for stabilization of HNE are comparable to previous studies (where stabilization of HNE with respect to water phase was ca. 4 kcal mol^{-1}), but flip flop barrier for HNE has been calculated to be significantly higher, around 6 kcal mol^{-1} (Vazdar et al., 2012b). However, in the previous study free energy profiles have been calculated using only a single HNE inserted in the membrane, whereas in this work we have a finite concentration of HNE in the membrane in the ratio of n(POPC):n(RA) = 10:1. The difference in calculated flip-flop barriers suggest that the flip-flop barrier is decreasing when RAs are present in the bilayer in a finite concentration due to their mutual interaction.

Free energy calculations show that the most lipophilic RA is NA, as can be expected from its structure where only one carbonyl group is present together with a fully saturated carbon chain. NE has also only one polar group, but is slightly less lipophilic due to one double bond in the carbon chain. HNE and ONE have two polar groups, but HNE is

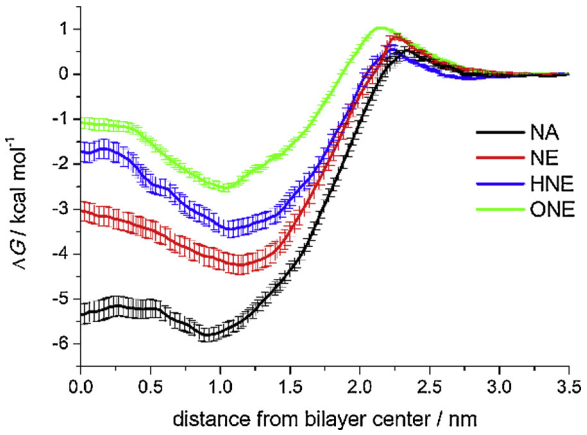

Fig. 6. Free energy profiles for translocation of NA (black), NE (red), HNE (blue) and ONE (green) across POPC bilayer.

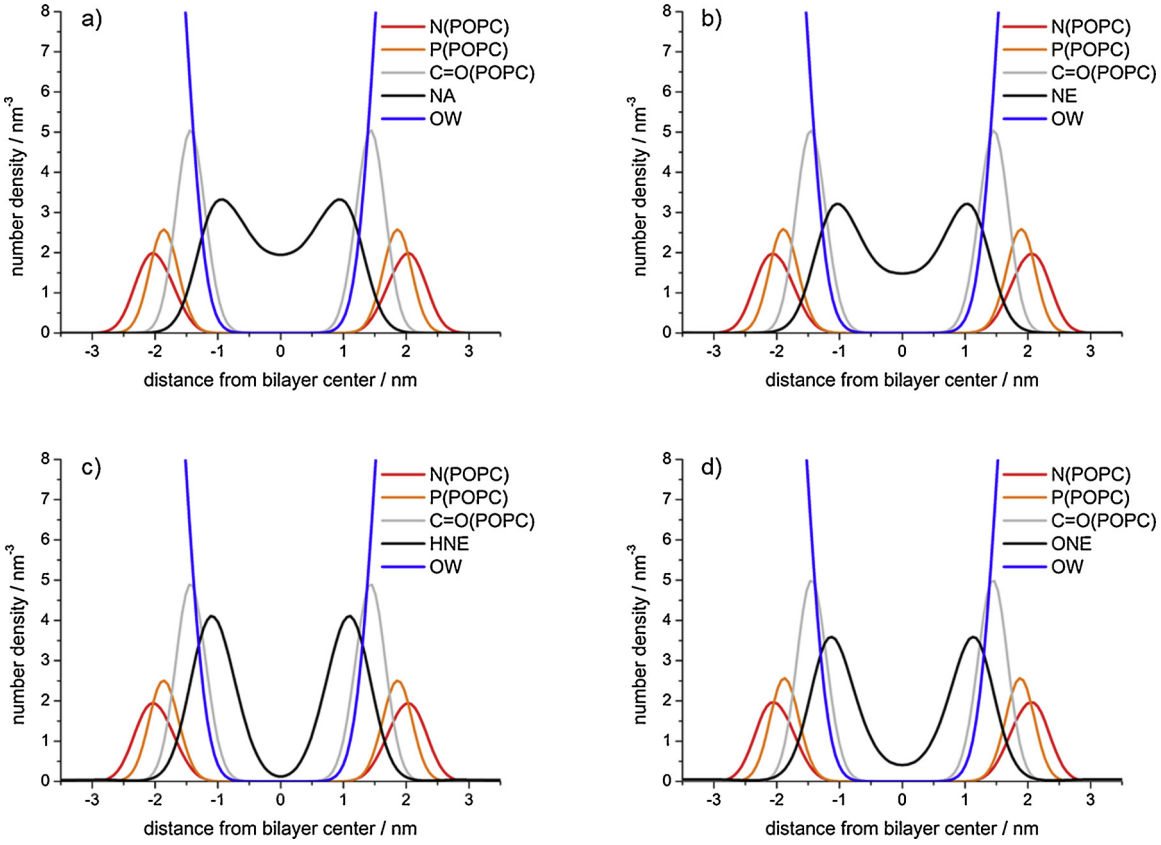

Fig. 5. Calculated number density profiles for lipid bilayer membranes: a) POPC + NA, b) POPC + NE, c) POPC + HNE, d) POPC + ONE. Number densities of nitrogen atom in POPC choline group (red), phosphorus atom of POPC phosphate group (orange), carbon atoms of POPC carbonyl group (grey), reactive aldehyde (black) and oxygen water atom (blue), are shown with respect to the distance from the bilayer center.

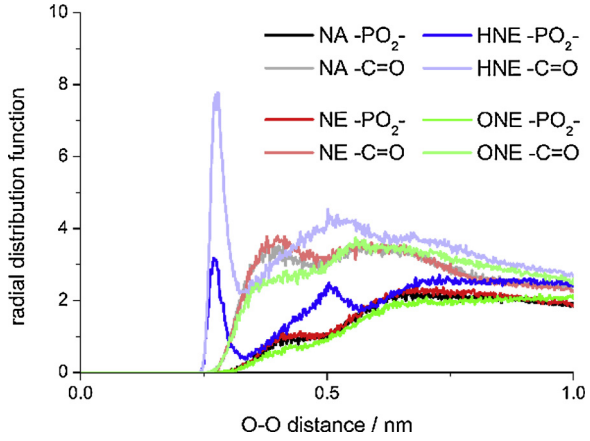

Fig. 7. Radial distribution functions (RDFs) for interaction between oxygen atoms in aldehyde group of NA (black and grey) and NE (red and light red), hydroxyl group of HNE (blue and light blue) and keto group of ONE (green and light green) vs corresponding oxygen atom in carbonyl group of POPC and phosphate group of POPC, respectively.

more lipophilic due to ability to make hydrogen bonds to carbonyl and phosphate POPC groups in contrast to ONE. The ability of HNE to act as a hydrogen bond donor is also reflected in the largest flip-flop barrier in the series, since the breaking of hydrogen bonds and translocation to the other leaflet has an additional energy penalty. The equilibrium position of all RAs center of mass is in the region of 1.0–1.2 nm from the bilayer center, just below POPC carbonyl groups (see Fig. 5). Additionally, MD simulations reveal another interesting fact – namely, the insertion of RAs from water to the phospholipid bilayers is not a spontaneous process and the free energy barrier for lipid insertion assumes values of 0.5–1.0 kcal mol^{-1}, with the largest barrier observed for ONE.

Finally, we analyze the hydrogen bonding pattern between polar groups of RAs, in particular the aldehyde group of NA, NE, hydroxyl group of HNE and keto group of ONE (Fig. 1), with POPC phosphate and carbonyl groups. The radial distribution functions (RDFs) of RA polar groups vs oxygen atom in carbonyl group of POPC and oxygen atoms in phosphate group of POPC, respectively, are presented in Fig. 7.

We see that HNE makes hydrogen bonds to POPC carbonyl and phosphate groups since the first RDF maximum is sharp and located at the distance between two corresponding oxygen atoms of ca 0.25 nm. Interestingly, the hydrogen bond towards carbonyl group is stronger than to phosphate as witnessed by an increased maximum in the corresponding RDF (Fig. 7). This is not intuitively anticipated, since the charge of oxygen atoms in phosphate groups is more negative than the corresponding charge on oxygen atoms in carbonyl groups. Therefore, a stronger electrostatic interaction between positively charged hydrogen atom in −OH group of HNE and oxygen atoms from POPC phosphate groups is expected. However, since POPC carbonyl groups are located deeper in the bilayer than phosphate groups, they are surrounded with less water allowing them to create hydrogen bonds to HNE which itself is located closer to POPC carbonyl than POPC phosphate groups (Fig. 5). This is an interesting phenomenon, showing that a balance of hydrogen bonding to water and HNE depends not only to the electrostatic interaction between HNE and polar lipid groups (and which should be stronger for POPC phosphate group), but also depends on the degree of solvation of polar lipid groups.

In the case of other RAs, they do not make hydrogen bonds to POPC as witnessed by the first RDF maximum which is found at distances larger than 0.35 nm between the corresponding oxygen atoms. Also, polar groups are more frequently found closer to carbonyl group than phosphate group as indicated by the larger first maximum in RDFs, being around 4 for interaction with POPC carbonyl and around 1 for interaction with POPC phosphate groups, which is expected due to their equilibrium position in the bilayer.

4. Discussion and conclusions

In this work, we studied behavior of a series of reactive aldehydes with POPC (Fig. 1), one of the most common phospholipids found in cellular membranes (van Meer et al., 2008), using FTIR spectroscopic experiments assisted with molecular dynamics simulations. Since the oxidative damage results from subsequent reactions of embedded RAs with surrounding lipids/proteins (Schaur, 2003), it is important to understand what occurs prior to the reactions themselves, i.e., how RAs are distributed in the membrane heterogeneous environment. In particular, we are interested in finding whether relatively small changes in the RA structure used in this work influence local phospholipid behavior and whether these differences can be monitored by FTIR spectroscopic experiments supplemented with the atomistic data.

With the intention of understanding the molecular details of the described interactions, we first employed FTIR spectroscopic measurements of RAs in POPC with the special emphasis to carbonyl stretching of POPC and RAs, as well as phosphate stretching of POPC. In the case of NA, the FTIR experimental results show that NA has carbonyl stretching spectra similar to single NA molecule in nonpolar C_2Cl_4 suggesting that NA is located in a similar nonpolar environment in the POPC bilayer. This is also evident in the EPR spectra which shows the largest increase in fluidity of POPC bilayer at the position of 5-DSPC probe when NA is added (Fig. 1) due to the largest residence time of NA around the probe disturbing native bilayer environment. These results are in excellent agreement with molecular dynamics simulations and free energy calculations which are showing that NA is the most lipophilic RA in the series, with the stabilization energy of ca -6 kcal mol^{-1}, and the lowest flip-flop barrier of ca. 0.5 kcal mol^{-1} indicating frequent flip-flop events which are the reason for the largest increase in bilayer fluidity around the EPR spin probe.

Upon going to NE, the FTIR data describing carbonyl stretching of NE, and in particular the second derivative analysis of the FTIR spectra of POPC carbonyl groups, shows that NE is located in two slightly different polar environments. A significant ratio of NE is bound to interfacial water and is therefore located closer to the membrane interface than NA, as indicated by the equilibrium position of NE (Fig. 6). These results are also supported by EPR measurements, which show that the disorder resulting from NE insertion is not as large as in the case of NA and it is relatively similar to neat POPC. The experimental results are corroborated by MD simulations which show that NE is less stable than NA in the bilayer, assuming value of ca. -4 kcal mol^{-1} with slightly increased flip-flop barrier than NA, being ca. 1 kcal mol^{-1}.

Going further in the series, the results show that HNE, as the only hydrogen bond donor of all studied RAs (Fig. 1), makes hydrogen bonding with available hydrogen bond acceptors (such as water, another HNE molecule or POPC carbonyl group). This is witnessed by a low frequency shift of $\nu(C = O_{HNE})$ band of about 15 cm^{-1} in comparison to single HNE in nonpolar C_2Cl_4 and a high frequency shift of $\nu(C = O_{POPC})$ band of 1 cm^{-1} (Fig. 2). This occurs mainly due to the interaction of HNE molecules between themselves, but a substantial portion of HNE species nevertheless make hydrogen bonds with carbonyl and phosphate groups of POPC (Fig. 7). It is interesting, however, that hydrogen bond is significantly stronger upon interaction of HNE with less electronegative carbonyl group of POPC than more electronegative phosphate group of POPC, as HNE is more closely situated being to POPC carbonyl groups in the bilayer. A detailed analysis of second derivative spectra of carbonyl stretching also shows that ratio of hydrogen bonded C=O groups of POPC is decreased at the expense of non-hydrogen bonded groups showing that HNE is replacing water around POPC carbonyl groups, but is not as efficient as a hydrogen bonding donor compared to water. Additionally, the phosphate stretching $\nu_{as}PO_2^-$ also shows a slight high-frequency shift, in contrast to other studied RAs. The effect of HNE insertion is also somewhat

visible in the EPR spectra, with order parameter *S* being slightly lower compared to NE, but within the error bar (Fig. 4). MD simulation data show that HNE is not as strongly stabilized in the membrane as NE (with the slightly higher stabilization energy of ca. -3.5 kcal mol^{-1}). However, the largest differences compared to other RAs are visible in the flip-flop free energy of HNE, assuming values of ca. 2 kcal mol^{-1}, which is larger than other values of the investigated series. This increase in flip-flop energy can be attributed to the energy penalty needed for breaking the hydrogen bonds between −OH group in HNE with carbonyl and/or phosphate groups of POPC.

As a final example in the series, ONE has two carbonyl groups via which it can interact which is visible in the FTIR spectra as two separate signals participating in hydrogen bonding to surrounding water. In the EPR spectra, the order parameter is the largest in the series (together with NE), showing the lowest influence on the disorder of the bilayer and bilayer fluidity when ONE is inserted is almost not changed compared to neat POPC. This data was confirmed as well with MD simulations, where we observe that ONE is stabilized by ca. -2.5 kcal mol^{-1} (Fig. 6) and does not participate in hydrogen bonding to carbonyl and phosphate groups of POPC. Interestingly, the free energy barrier for entrance of ONE to the POPC bilayer is around 1 kcal mol^{-1} (Fig. 6), which is slightly higher compared to other studied RAs, due to presence of two carbonyl groups which cannot get stabilized by the hydrogen bonding to phosphate and carbonyl POPC groups upon insertion into the bilayer.

In conclusion, we described by a combination of spectroscopic techniques and molecular dynamics simulations the detailed interactions between different RAs and POPC phospholipid bilayers. It is important to note that by using FTIR spectroscopy with atomistic data, the level of molecular details which can be extracted and analyzed is far superior when compared to FTIR spectroscopy or MD simulations alone. We demonstrated that even minute changes in the structures of reactive aldehydes (Fig. 1) leave the unique molecular fingerprint which can be monitored by vibrational spectroscopy and analyzed with the help of molecular dynamics simulations. In particular, we showed that carbonyl group of POPC is an excellent probe for studying interactions with compounds where hydrogen bonding is essential, such as reactive aldehydes studied in this work. Although phosphate group is also a possible target for FTIR analysis, it was shown by second order FTIR analysis that it is not as sensitive as carbonyl group for hydrogen bonding monitoring of RAs, due to the fact that RAs make more hydrogen bonds with POPC carbonyl group than POPC phosphate group. Incidentally, we do not expect any qualitative changes in the interactions of RAs with lipid when POPC is in the liquid crystalline phase. In contrast to measurements around lipid melting point T_m (which are frequently used in other IR and DSC temperature studies where significant changes in the spectra is routinely observed) the differences in the aldehyde IR signal with temperature are expected to be very small and hard to be detected.

Finally, we should mention that systems studied in this work are a benchmark for future combined experimental/atomistic characterization of more realistic lipid bilayers under oxidative stress. In particular, we plan to use reactive lipids, such as phosphoethanolamine (PE) together with embedded peptides/proteins, which can both react with different reactive aldehydes leading to deleterious changes of the phospholipid structure with important consequences on stability of biological membranes. Moreover, we should also stress that in realistic bilayers, POPC (or any other constitutive lipids) are prone to oxidation themselves by ambient free radicals, resulting in variously oxidized lipids. This will have an effect on the interactions of RAs with the modified lipids, which can be quite different from the interaction of RAs with intact lipids. Altogether, we believe that the presented combination of the experimental techniques and molecular dynamics simulations represents a promising tool for studying oxidative stress at the molecular level in the future.

Acknowledgment

This study was supported by Croatian Science Foundation, Projects No. UIP-2014-09-6090 and IP-2018-01-3168. We thank the computer cluster Isabella based in SRCE - University of Zagreb, University Computing Centre for computational resources. D. B. and K. V. acknowledge the financial support from Croatian Academy of Sciences and Arts. Authors thank to Dr. Marina Ilakovac Kveder for helpful discussions and Dr. Suzana Šegota for instrumental support.

References

Abraham, M.J., Murtola, T., Schulz, R., Pall, S., Smith, J.C., Hess, B., Lindah, E., 2015. Gromacs: high performance molecular simulations through multi-level parallelism from laptops to supercomputers. SoftwareX 1–2, 19–25. https://doi.org/10.1016/j.softx.2015.06.001.

Bayly, C.I., Cieplak, P., Cornell, W., Kollman, P.A., 1993. A well-behaved electrostatic potential based method using charge restraints for deriving atomic charges: the RESP model. J. Phys. Chem. 97, 10269–10280. https://doi.org/10.1021/j100142a004.

Casal, H.L., Mantsch, H.H., 1984. Polymorphic phase behaviour of phospholipid membranes studied by infrared spectroscopy. BBA - Rev. Biomembr. https://doi.org/10.1016/0304-4157(84)90017-0.

Casal, H.L., Mantsch, H.H., Hauser, H., 1987. Infrared studies of fully hydrated saturated phosphatidylserine bilayers. Effect of Li + and Ca2 +. Biochemistry 26, 4408–4416. https://doi.org/10.1021/bi00388a033.

Catala, A., 2009. Lipid peroxidation of membrane phospholipids generates hydroxy-alkenals and oxidized phospholipids active in physiological and/or pathological conditions. Chem. Phys. Lipids 157, 1–11.

Choi, S., Swanson, J.M., 1995. Interaction of cytochrome c with cardiolipin: an infrared spectroscopic study. Biophys. Chem. 54, 271–278. https://doi.org/10.1016/0301-4622(94)00151-9.

Cieślik-Boczula, K., Maniewska, J., Grynkiewicz, G., Szeja, W., Koll, A., Hendrich, A.B., 2012. Interaction of quercetin, genistein and its derivatives with lipid bilayers - an ATR IR-spectroscopic study. Vib. Spectrosc. 62, 64–69. https://doi.org/10.1016/j.vibspec.2012.05.010.

Désormeaux, A., Laroche, G., Pézolet, M., Bougis, P.E., 1992. Characterization by infrared spectroscopy of the interaction of a cardiotoxin with phosphatidic acid and with binary mixtures of phosphatidic acid and phosphatidylcholine. Biochemistry 31, 12173–12182. https://doi.org/10.1021/bi00163a029.

Díaz, S.B., Biondi de Lopez, A.C., Disalvo, E.A., 2003. Dehydration of carbonyls and phosphates of phosphatidylcholines determines the lytic action of lysoderivatives. Chem. Phys. Lipids 122, 153–157. https://doi.org/10.1016/S0009-3084(02)00186-X.

Essmann, U., Perera, L., Berkowitz, M.L., Darden, T., Lee, H., Pedersen, L.G., 1995. A smooth particle mesh Ewald method. J. Chem. Phys. 103, 8577–8593. https://doi.org/10.1063/1.470117.

Esterbauer, H., Schaur, R.J., Zollner, H., 1991. Chemistry and Biochemistry of 4-hydroxynonenal, malonaldehyde and related aldehydes. Free Radic. Biol. Med. 11, 81–128.

Feller, S.E., 2000. Molecular dynamics simulations of lipid bilayers. Curr. Opin. Colloid Interface Sci. 5, 217–223. https://doi.org/10.1016/S1359-0294(00)00058-3.

Fringeli, U.P., Günthard, H.H., 1981. Infrared membrane spectroscopy. Mol. Biol. Biochem. Biophys. 31, 270–332.

Grdadolnik, J., Hadži, D., 1993. Conformational effects of metal salt binding to the polar head of phosphatidylcholines investigated by FTIR spectroscopy. Chem. Phys. Lipids 65, 121–132. https://doi.org/10.1016/0009-3084(93)90045-5.

Gruenbaum, S.M., Skinner, J.L., 2011. Vibrational spectroscopy of water in hydrated lipid multi-bilayers. I. Infrared spectra and ultrafast pump-probe observables. J. Chem. Phys. 135. https://doi.org/10.1063/1.3615717.

Grune, T., Davies, K.J.A., 2003. The proteasomal system and HNE-modified proteins. Mol. Aspects Med. 24, 195–204.

Guichardant, M., Taibi-Tronche, P., Fay, L.B., Lagarde, M., 1998. Covalent modifications of aminophospholipids by 4-hydroxynonenal. Free Radic. Biol. Med. 25, 1049–1056. https://doi.org/10.1016/S0891-5849(98)00149-X.

Hess, B., Bekker, H., Berendsen, H.J.C., Fraaije, J.G.E.M., 1997. LINCS: a linear constraint solver for molecular simulations. J. Comp. Chem. 18, 1463–1472.

Hub, J.S., De Groot, B.L., Van Der Spoel, D., 2010. G-whams-a free Weighted Histogram Analysis implementation including robust error and autocorrelation estimates. J. Chem. Theory Comput. 6, 3713–3720. https://doi.org/10.1021/ct100494z.

Hull, M.C., Cambrea, L.R., Hovis, J.S., 2005. Infrared spectroscopy of fluid lipid bilayers. Anal. Chem. 77, 6096–6099. https://doi.org/10.1021/ac050990c.

Jämbeck, J.P.M., Lyubartsev, A.P., 2012a. Another piece of the membrane puzzle: extending slipids further. J. Chem. Theory Comput. 9, 774–784. https://doi.org/10.1021/ct300777p.

Jämbeck, J.P.M., Lyubartsev, A.P., 2012b. An extension and further validation of an all-atomistic force field for biological membranes. J. Chem. Theory Comput. 8, 2938–2948. https://doi.org/10.1021/ct300342n.

Jämbeck, J.P.M., Lyubartsev, A.P., 2012c. Derivation and systematic validation of a refined all-atom force field for phosphatidylcholine lipids. J. Phys. Chem. B 116, 3164–3179. https://doi.org/10.1021/jp212503e.

Jorgensen, W.L., Chandrasekhar, J., Madura, J.D., Impey, R.W., Klein, M.L., 1983. Comparison of simple potential functions for simulating liquid water. J. Chem. Phys. 79, 926–935. https://doi.org/10.1063/1.445869.

Jovanović, O., Pashkovskaya, A.A., Annibal, A., Vazdar, M., Burchardt, N., Sansone, A., Gille, L., Fedorova, M., Ferreri, C., Pohl, E.E., 2015. The molecular mechanism behind reactive aldehyde action on transmembrane translocations of proton and potassium ions. Free Radic. Biol. Med. 89, 1067–1076. https://doi.org/10.1016/j.freeradbiomed.2015.10.422.

Kim, Y.A., Tarahovsky, Y.S., Yagolnik, E.A., Kuznetsova, S.M., Muzafarov, E.N., 2013. Lipophilicity of flavonoid complexes with iron(II) and their interaction with liposomes. Biochem. Biophys. Res. Commun. 431, 680–685. https://doi.org/10.1016/j.bbrc.2013.01.060.

Klauda, J.B., Venable, R.M., Freites, J.A., O'Connor, J.W., Tobias, D.J., Mondragon-Ramirez, C., Vorobyov, I., MacKerell, A.D., Pastor, R.W., 2010. Update of the CHARMM all-atom additive force field for lipids: validation on six lipid types. J. Phys. Chem. B 114, 7830–7843. https://doi.org/10.1021/jp101759q.

Kuć, M., Cieślik-Boczula, K.,-wiątek, P., Jaszczyszyn, A., Gąsiorowski, K., Malinka, W., 2015. FTIR-ATR study of the influence of the pyrimidine analog of fluphenazine on the chain-melting phase transition of sphingomyelin membranes. Chem. Phys. 458, 9–17. https://doi.org/10.1016/j.chemphys.2015.06.010.

Lewis, R.N.A.H., McElhaney, R.N., 2013. Membrane lipid phase transitions and phase organization studied by Fourier transform infrared spectroscopy. Biochim. Biophys. Acta Biomembr. https://doi.org/10.1016/j.bbamem.2012.10.018.

Lewis, R.N.A.H., McElhaney, R.N., 2007. Fourier transform infrared spectroscopy in the study of lipid phase transitions in model and biological membranes. In: Dopico, A.M. (Ed.), Methods in Membrane Lipids. Humana Press, Totowa, NJ, pp. 207–226. https://doi.org/10.1007/978-1-59745-519-0_14.

Lewis, R.N.A.H., Pohle, W., McElhaney, R.N., 1996. The interfacial structure of phospholipid bilayers: Differential scanning calorimetry and Fourier transform infrared spectroscopic studies of 1,2-dipalmitoyl-sn-glycero-3-phosphorylcholine and its dialkyl and acyl-alkyl analogs. Biophys. J. 70, 2736–2746. https://doi.org/10.1016/S0006-3495(96)79843-0.

Malingriaux, E.A., Rupprecht, A., Gille, L., Jovanovic, O., Jezek, P., Jaburek, M., Pohl, E.E., 2013. Fatty acids are key in 4-hydroxy-2-nonenal-mediated activation of uncoupling proteins 1 and 2. PLoS One 8, e77786. https://doi.org/10.1371/journal.pone.0077786.

Mannock, D.A., Lewis, R.N.A.H., McElhaney, R.N., 2006. Comparative calorimetric and spectroscopic studies of the effects of lanosterol and cholesterol on the thermotropic phase behavior and organization of dipalmitoylphosphatidylcholine bilayer membranes. Biophys. J. 91, 3327–3340. https://doi.org/10.1529/biophysj.106.084368.

Marinov, R., Dufourc, E.J., 1996. Thermotropism and hydration properties of POPE and POPE-cholesterol systems as revealed by solid state2H and31P-NMR. Eur. Biophys. J. 24, 423–431. https://doi.org/10.1007/BF00576714.

Marsh, D., 1981. Electron Spin Resonance: Spin labels., Molecular Biology, Biochemistry, and Biophysics. Springer, Berlin, Heidelberg.

Menges, F., 2018. Spectragryph - Optical Spectroscopy Software.

Mirosavljević, K., Matković, M., Mlinarić-Majerski, K., Noethig-Laslo, V., 2014. Effect of adamantyl compounds on dynamics of spin labelled multilamellar liposomes. Croat. Chem. Acta 87, 249–253. https://doi.org/10.5562/cca2399.

Mirosavljević, K., Noethig-Laslo, V., 2008. Spin labelling study of interfacial properties of egg-phosphatidylcholine liposomes as a function of cholesterol concentrations. Chem. Phys. Lipids 155, 74–79. https://doi.org/10.1016/j.chemphyslip.2008.07.006.

Miyamoto, S., Kollman, P.A., 1992. Settle: an analytical version of the SHAKE and RATTLE algorithm for rigid water models. J. Comp. Chem. 13, 962.

Moradi, S., Nowroozi, A., Shahlaei, M., 2019. Shedding light on the structural properties of lipid bilayers using molecular dynamics simulation: a review study. RSC Adv. 9, 4644–4658. https://doi.org/10.1039/C8RA08441F.

Morse, P.D., 1987. Thirty-first annual meeting 22–26 February 1987 Rivergate Convention Center, New Orleans, Louisiana. Biophys. J. 51, 440a–495a. https://doi.org/10.1016/S0006-3495(87)83355-6.

Nosé, S., 1984. A molecular dynamics method for simulations in the canonical ensemble. Mol. Phys. 52, 255–268. https://doi.org/10.1080/00268978400101201.

Parrinello, M., Rahman, A., 1981. Polymorphic transitions in single crystals: a new molecular dynamics method. J. Appl. Phys. 52, 7182–7190. https://doi.org/10.1063/1.328693.

Pawlikowska-Pawlęga, B., Dziubińska, H., Król, E., Trębacz, K., Jarosz-Wilkołazka, A., Paduch, R., Gawron, A., Gruszecki, W.I., 2014. Characteristics of quercetin interactions with liposomal and vacuolar membranes. Biochim. Biophys. Acta Biomembr. 1838, 254–265. https://doi.org/10.1016/j.bbamem.2013.08.014.

Petrus, J., Czarnik-Matusewicz, B., Petrus, R., Cieślik-Boczula, K., Jaszczyszyn, A., Gąsiorowski, K., 2015. Fluphenazine: from an isolated molecule to its interaction with lipid bilayers. Chem. Phys. Lipids 186, 51—60. https://doi.org/10.1016/j.chemphyslip.2015.01.002.

Ryu, S.R., Noda, I., Jung, Y.M., 2010. What is the origin of positional fluctuation of spectral features: true frequency shift or relative intensity changes of two overlapped bands? Appl. Spectrosc. 64, 1017–1021. https://doi.org/10.1366/000370210792434396.

Schaur, R.J., 2003. Basic aspects of the biochemical reactivity of 4-hydroxynonenal. Mol. Aspects Med. 24, 149–159.

Šegota, S., Vojta, D., Kendziora, D., Ahmed, I., Fruk, L., Baranović, G., 2015a. Ligand-dependent nanoparticle clustering within lipid membranes induced by surrounding medium. J. Phys. Chem. B 119, 5208–5219. https://doi.org/10.1021/acs.jpcb.5b00898.

Šegota, S., Vojta, D., Pletikapić, G., Baranović, G., 2015b. Ionic strength and composition govern the elasticity of biological membranes. A study of model DMPC bilayers by force- and transmission IR spectroscopy. Chem. Phys. Lipids 186, 17–29. https://doi.org/10.1016/j.chemphyslip.2014.11.001.

Seon Hwa, L., Oe, T., Blair, I.A., 2001. Vitamin C-induced decomposition of lipid hydroperoxides to endogenous genotoxins. Science (80-.) 292, 2083–2086. https://doi.org/10.1126/science.1059501.

Singh, U.C., Kollman, P.A., 1984. An approach to computing electrostatic charges for molecules. J. Comput. Chem. 5, 129–145. https://doi.org/10.1002/jcc.540050204.

Škulj, S., Vazdar, K., Margetić, D., Vazdar, M., 2019. Revisited Mechanism of reaction between model lysine amino acid side chain and 4-hydroxynonenal in different solvent environments. J. Org. Chem. 84, 526–535.

Soulère, L., Queneau, Y., Doutheau, A., 2007. An expeditious synthesis of 4-hydroxy-2E-nonenal (4-HNE), its dimethyl acetal and of related compounds. Chem. Phys. Lipids 150, 239–243. https://doi.org/10.1016/j.chemphyslip.2007.07.003.

Tamm, L.K., Tatulian, S.A., 1997. Infrared spectroscopy of proteins and peptides in lipid bilayers. Q. Rev. Biophys. 30, 365–429. https://doi.org/10.1017/S0033583597003375.

Tatulian, S.A., 2003. Attenuated total reflection fourier transform infrared spectroscopy: a method of choice for studying membrane proteins and lipids. Biochemistry 42, 11898–11907. https://doi.org/10.1021/bi034235+.

Tieleman, D.P., Marrink, S.J., Berendsen, H.J.C., 1997. A computer perspective of membranes: molecular dynamics studies of lipid bilayer systems. Biochim. Biophys. Acta - Rev. Biomembr. 1331, 235–270. https://doi.org/10.1016/S0304-4157(97)00008-7.

van Meer, G., Voelker, D.R., Feigenson, G.W., 2008. Membrane lipids: where they are and how they behave. Nat. Rev. Mol. Cell Biol. 9, 112–124.

Vazdar, K., Vojta, D., Margetić, D., Vazdar, M., 2017. Reaction mechanism of covalent modification of phosphatidylethanolamine lipids by reactive aldehydes 4-hydroxy-2-nonenal and 4-oxo-2-nonenal. Chem. Res. Toxicol. 30, 840–850. https://doi.org/10.1021/acs.chemrestox.6b00443.

Vazdar, M., Jurkiewicz, P., Hof, M., Jungwirth, P., Cwiklik, L., 2012a. Behavior of 4-hydroxynonenal in phospholipid membranes. J. Phys. Chem. B 116, 6411–6415. https://doi.org/10.1021/jp3044219.

Vazdar, M., Jurkiewicz, P., Hof, M., Jungwirth, P., Cwiklik, L., 2012b. Behavior of 4-hydroxynonenal in phospholipid membranes. J. Phys. Chem. B 116, 6411–6415.

Veiga, M.P., Arrondo, J.L.R., Goñi, F.M., Alonso, A., 1999. Ceramides in phospholipid membranes: effects on bilayer stability and transition to nonlamellar phases. Biophys. J. 76, 342–350. https://doi.org/10.1016/S0006-3495(99)77201-2.

Wong, P.T.T., Mantsch, H.H., 1988. High-pressure infrared spectroscopic evidence of water binding sites in 1,2-diacyl phospholipids. Chem. Phys. Lipids 46, 213–224. https://doi.org/10.1016/0009-3084(88)90024-2.

Yin, H., Xu, L., Porter, N.A., 2011. Free radical lipid peroxidation: mechanisms and analysis. Chem. Rev. 111, 5944–5972.

Žarković, N., Čipak, A., Jaganjac, M., Borović, S., Žarković, K., 2013. Pathophysiological relevance of aldehydic protein modifications. J. Proteomics. https://doi.org/10.1016/j.jprot.2013.02.004.

Zimmermann, L., Moldzio, R., Vazdar, K., Krewenka, C., Pohl, E.E., 2017. Nutrient deprivation in neuroblastoma cells alters 4-hydroxynonenal-induced stress response. Oncotarget 8, 8173–8188. https://doi.org/10.18632/oncotarget.14132.